Front. Mater. Sci. China 2009, 4(1): 310–318
DOI 10.1007/s11706-009-0021-4

RESEARCH ARTICLE

Synthesis, characterization and annealing of mechanically alloyed nanostructured FeAl powder

M. M. RAJATH HEGDE (✉), A. O. SURENDRANATHAN

Department of Metallurgical and Materials Engineering, NITK Surathkal, Srinivasanagar-575025, Dakshina Kannada, Karnataka, India

Abstract Elemental powders of Fe and Al were mechanically alloyed using a high energy rate ball mill. A nanostructure disordered Fe(Al) solid solution was formed at an early stage. After 28 h of milling, it was found that the Fe(Al) solid solution was transformed into an ordered FeAl phase. During the entire ball milling process, the elemental phase co-existed with the alloyed phase. Ball milling was performed under toluene to minimise atmospheric contamination. Ball milled powders were subsequently annealed to induce more ordering. Phase transformation and structural changes during mechanical alloying (MEA) and subsequent annealing were investigated by X-ray diffraction (XRD). Scanning electron microscope (SEM) was employed to examine the morphology of the powders and to measure the powder particle size. Energy dispersive spectroscopy (EDS) was utilised to examine the composition of mechanically alloyed powder particles. XRD and EDS were also employed to examine the atmospheric and milling media contamination. Phase transformation at elevated temperatures was examined by differential scanning calorimeter (DSC). The crystallite size obtained after 28 h of milling time was around 18 nm. Ordering was characterised by small reduction in crystallite size while large reduction was observed during disordering. Micro hardness was influenced by Crystallite size and structural transformation.

Keywords nanostructured powder, mechanical alloying, FeAl, disorder, order

1 Introduction

The FeAl intermetallic compound possesses advantageous properties, in particular, a high specific strength (strength to density ratio), high specific stiffness, good strength at intermediate temperatures, an excellent corrosion resistance at elevated temperatures under oxidizing, carburizing and sulfidizing atmospheres, with relatively high electrical resistivity and low thermal conductivity [1–4]. These features make the FeAl intermetallics compound a very attractive material for structural applications at elevated temperatures in hostile environments [3,4]. Moreover, Fe and Al, which are raw materials of the FeAl phase, are inexpensive. Additionally the FeAl intermetallic compound is lighter than steels or Ni-based alloys. Therefore, ordered FeAl alloys would be utilised as a substitute for stainless steels or Ni-based super alloys. However, in the FeAl compound, and likewise in the other intermetallic aluminides, the main drawback concerning their possible technological applications is its low ductility in the cast form at room temperatures and processing problems [3,4]. Mechanical alloying (MEA) is a widely used process for the synthesis of variety of alloys [5,6]. The MEA process leads to an alloy formation by solid state reactions assisted by severe plastic deformation that occurs during ball milling of the elemental powders. The MEA technique allows one to overcome problems such as large differences in melting points of the alloying components as well as unwanted segregation or evaporation that could occur during melting and casting. Usually the mechanically alloyed products possess nanocrystalline or amorphous structure [5,6]. Nanocrystalline materials are potentially attractive for many applications since the reduction of the grain size to the nanometer scale can improve their physical and mechanical properties [7,8]. Some properties, such as high strength and hardness [9,10], ductilisation of brittle materials [11,12] and enhanced diffusivity [13] that are superior to those of the conventional materials may result from the nanocrystalline structure.

In this work, we focus on the MEA of elemental powders of Fe and Al. MEA was achieved by high energy rate ball milling to obtain nanostructured Fe-50at.%Al alloy powders. The phase transformation, nanostructure, morphology, thermal stability and the thermal behaviour of

Received November 6, 2008; accepted December 16, 2008

E-mail: rajathhegdemm63@yahoo.co.in

the powders were investigated by XRD, SEM and DSC, respectively. Micro hardness test was conducted on the ball milled powders.

2 Experimental

2.1 Procedures

Elemental powders (purity of 99.5% and about 60 μm in size) of Fe and Al were ball milled using high energy rate planetary ball mill of the Retsch PM-100 type. The ball to powder weight ratio was 10:1. Tungsten carbide jar and balls were used and to minimise atmospheric contamination, milling process was carried out under toluene solution. The lid of the jar has an 'o' ring. The jar is filled with balls, elemental powders and the required quantity of toluene solution. The lid is placed firmly on the jar and the jar is then clamped securely inside the ball mill and is completely leak proof. Elemental powders were mechanically alloyed as a function of ball milling time and an average composition of about Fe-50at.%Al was obtained. The milling process was interrupted at certain time interval and a small quantity of powder was taken out for characterization.

The ball milled powders were subsequently annealed at temperatures ranging from 150°C to 450°C in a vacuum furnace evacuated down to 10^{-4} Torr ($\approx 1.33\times10^{-2}$ Pa). A reference sample was produced by annealing the mechanically alloyed powder at 900ºC for 2 h.

Phase transformation at elevated temperatures was investigated by a Shimadzu Differential Scanning Calorimeter (DSC-50). The powders were heated under flowing argon at a heating rate of 10°C/min in the temperature range from 30°C to 400°C.

The Vicker's micro hardness (VMH) indentation test was performed using a Clemex computer-controlled micro hardness tester. The powders were mounted in an epoxy cured at room temperature resin and were successively polished down to 0.3 μm. The test was carried out by applying a load of 10 gm on single powder particle. Each micro hardness value shown in the results are the average of at least 5 measurements on different particles.

2.2 Characterization

A Jeol X-ray diffractometer with a Cu Kα radiation (λ= 0.1542 nm) was utilised in investigating the structural and phase changes during the MEA of the elemental powders and subsequent annealing. Furthermore, the investigations into the atmospheric and milling media contaminations during MEA were also done by XRD.

The lattice parameters were determined using at least three higher angle 2θ peaks. The effective grain size, D, was calculated by averaging the results from applying the Scherrer formula (Eq. (1)) to the first three diffraction peaks:

$$\beta_{\text{crystallite}} = \frac{K\lambda}{D\cos\theta} \tag{1}$$

where K is the Scherrer constant, λ is the wavelength of the incident radiation and θ is the Bragg angle. β, the full width at half maximum (FWHM) of the peaks, was obtained by subtracting the instrumental broadening using a fully annealed sample, β_i, from the observed broadening, β_o, using Eq. (2) as follows:

$$\beta^2_{\text{crystllite}} = \beta^2_o - \beta^2_i \tag{2}$$

From XRD patterns, the relative long range order (LRO) parameter, S, was determined (Eq. (3)) by a comparison of the relative intensities of super lattice ($h+k+l=$ odd) and fundamental ($h+k+l=$ even) peaks of nano powders (28 h milled powder sample 221/110) with respect to the well annealed reference sample (100/110) according to Eq. (3) as follows:

$$S = \left[\frac{(I_s/I_f)_n}{(I_s/I_f)_r}\right]^{1/2} \tag{3}$$

where I_s is the integrated intensity of the superlattice reflection peak, I_f is the integrated intensity of the fundamental (110) peak, while 'n' and 'r' represent nano (28 h milled) and reference samples, respectively.

A Jeol 6380 analytical scanning electron microscope (SEM) was utilised in particle size measurements and to study the morphology of the mechanically alloyed powder samples.

The Energy dispersive X-ray spectroscopy (EDS) facility in the SEM was utilised to examine the chemical composition of the mechanically alloyed samples. The investigation into milling media and atmospheric contaminations were also done utilising the EDS facility.

3 Results and discussion

3.1 XRD results of ball milled samples

The XRD patterns for the samples ball milled for different durations are shown in Figs. 1–4. For the 1 h milled sample, the fcc Al (200), (220), (222), (400) and (420) peaks superpose upon the (110), (200), (211), (220) and (310) peaks of bcc Fe. The intensity of the Al (111) peak is highest and the Al (331) the least among all the peaks in the diffraction pattern as shown in Fig. 1. From Table 1, for the 1 h milled sample, the Bragg angle of the superposed (110/200) peak is slightly less than that of unmilled bcc Fe, whereas the lattice parameter (0.2870 nm) obtained from this peak is greater than that of the unmilled Fe. These results suggest the beginning of the phase transformation. The XRD pattern for 12 h milled sample from Fig. 2 shows the intensity of the strongest Al (111 and 311) peaks

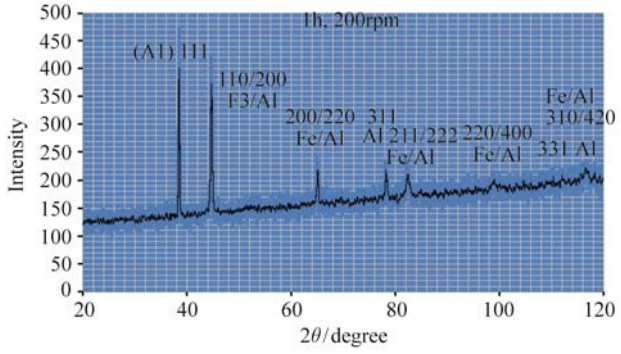

Fig. 1 XRD pattern of 1 h milled sample; fcc Al (111) peak has the highest intensity among all the peaks, while among the superposed peaks Fe/Al (110/200) has the highest intensity

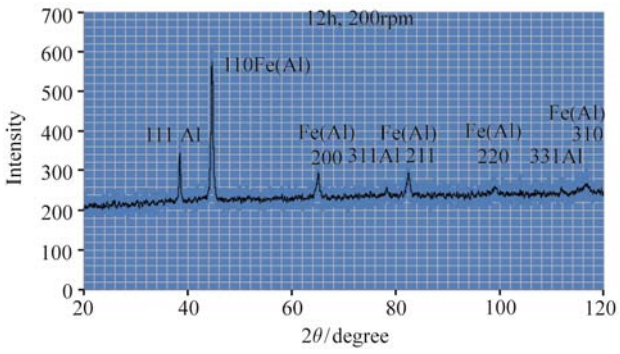

Fig. 2 XRD pattern of 12 h milled sample; the intensity of Al peaks decreased while that of fundamental peaks increased with peak broadening

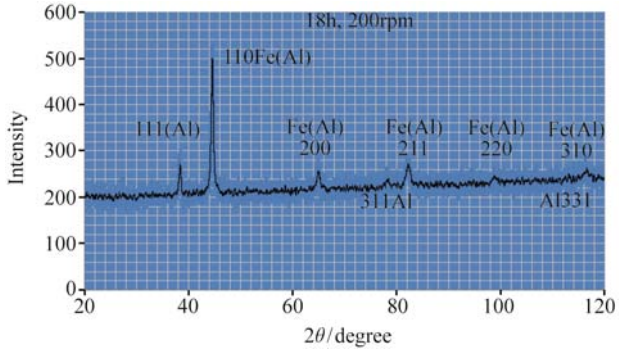

Fig. 3 XRD pattern of 18 h ball milled sample; decrease in intensity of Al peaks, fundamental peak broadening are further observed compared to the pattern of 12 h milled sample

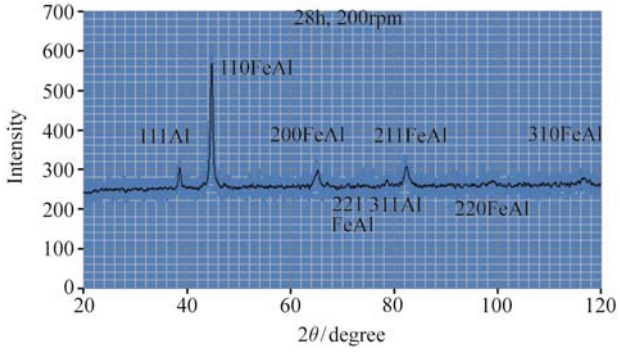

Fig. 4 Indexed XRD pattern of 28 h milled sample; low intensity bcc super lattice peak (221) is seen, further broadened fundamental peak and diminished Al peaks are observed, Al 331 peak is not seen

decreased compared to the pattern of one hr sample. The strongest Fe peak (110) becomes the most intense one, slightly asymmetric, broadened and appears at a slightly lower Bragg angle. The decrease in the intensity of Al peaks indicate the diffusion of fcc Al atoms into bcc α Fe lattice, simultaneously peak shifting to lower Bragg angles and asymmetric formation indicates the phase transformation from elemental phase to a disordered bcc Fe(Al) solid solution. Peak broadening is due to grain refinement, as seen from Table 1. The crystallite size reduces to around 22 nm. The intensity of bcc (110) peak is around 350 units, this increase in intensity compared to the pattern of 1 h milled sample suggests the strong prevalence of Fe(Al) phase at the expense of elemental phase, the bcc (110) peak of Fe(Al) solid solution is known as fundamental peak. Asymmetric broadening of Fe peaks is mainly due to the formation of Fe(Al) solid solution and the unit cell parameter of such bcc solid solution are higher than that of pure Fe, such similar observations are also mentioned [14], Table 1 indicates that the lattice parameter obtained is 0.2875 nm, which is greater than that of unmilled Fe and 1 h milled sample.

Table 1 XRD peaks and structural parameters for fundamental peaks and super lattice peak at different ball milling duration, contracted lattice parameter and crystallite size are 0.2869 and 18.32 nm respectively

milling time/h	2θ/degree	*hkl*	bcc/fcc	FeAl	space, *d*/nm	lattice parameter, *a*/nm	crystallite size, *D*/nm	fundamental/ super lattice peak
0	38.52	111	fcc	Al	–	0.4044	–	elemental
0	44.73	110	bcc	Fe	0.2024	0.2862	–	elemental
1	44.632	110/200	bcc/fcc	Fe/Al	0.2030	0.2870/0.4060	25.68	fundamental
12	44.56	110	bcc	Fe(Al)	0.2033	0.2875	22.44	fundamental
18	44.5	110	bcc	Fe(Al)	0.2036	0.2879	19.95	fundamental
28	44.656	110	bcc	FeAl	0.2029	0.2869	18.32	fundamental
28	71.308	221/300	bcc	FeAl	–	–	–	super lattice

As the milling time increases, separate Fe and Al phases are being replaced by a bcc Fe(Al) solid solution, hence the peaks corresponding to bcc Fe(Al) solid solution, the fundamental peaks ($h + k + l =$ even) are visible with greater intensities than the Al peaks as shown in Fig. 3 for 18 h milled sample. Figure 3 also shows fundamental peak broadening, shifting to a lower Bragg angle and the absence of super lattice reflection ($h + k + l =$ odd). Peak shifting to a lower Bragg angle as a result of milling time, points to an expansion of the bcc Fe lattice (0.2879 nm) during the alloying process as indicated in Table 1. Lattice expansion introduces antisite defects during the disorder as a result of milling time [15], i.e., both Fe and Al atoms are able to substitute each other's lattice, and the crystallite size obtained at the end of 18 h of milling is 19.95 nm. The absence of super lattice reflection proves the disordered structure of the solid solution. Sebastian et al. [16] have observed such variations in peak intensities, shift in the Bragg angle, peak broadening and asymmetric formation and have interpreted it to be due to the migration of Al into Fe, formation of bcc Fe(Al) solid solution (A2) and crystallite size refinement.

Further diminishing of Al peaks, fundamental peak broadening and shift to higher Bragg angle are noticed for 28 hrs of milled sample as shown in Fig. 4. Observe the vanishing of Al (331) peak and the emergence of a low intensity bcc super lattice peak (221). These results indicate the transition from bcc Fe(Al) solid solution of the disordered phase to the FeAl ordered phase. The ordering phenomenon reduces the lattice parameter (0.2869 nm) and shifts the peak to higher Bragg angle as observed from the Table 1. The lattice contraction is due to annihilation of the antisite defects resulting from diffusion over short distances and increased short range order [17]. From the XRD data of the reference sample and the 28 h sample, the LRO parameter, S, is 0.49, indicates that the mechanically alloyed sample is partially ordered. Morris-Munoz et al. [18] have shown the formation of a partially ordered FeAl phase at longer milling duration. The presence of elemental Al peak during the MEA process as a result of ball milling indicates the prevalence of two phases (the elemental phase co-exists with the alloyed phase).

The absence of Fe_3Al (DO_3) peak around the Bragg angle of 26° in the XRD pattern confirms that the nanoparticle sample does not contain significant contamination from oxygen during the processing, furthermore, none of the XRD patterns show peaks of tungsten and carbon, suggesting negligible contamination from the milling media.

The lattice parameter increases from 0.2862 nm for unmilled Fe to 0.2879 nm for 18 h milled sample. This lattice expansion is shown in Fig. 5(a). It is due to the formation of disordered Fe(Al) as explained earlier. The lattice contraction is accompanied by a transformation to an ordered FeAl phase. One of the possible reasons for fundamental peak broadening is crystallite size refinement, (Fig. 5(b)). Lattice contraction is characterised by a marginal decrease in crystallite size (from 19.95 to 18.32 nm) as compared to a large reduction (from 25.68 to 19.95 nm) during lattice expansion. In Fig. 5(c), the crystallite size decrease is steep during the milling time from 12 to 18 h. It is due to the disordered phase which prevails during MEA at this juncture. During disordering, the lattice expansion occurs, the entropy of the system is dominant and the atoms are located randomly in the bcc lattice of Fe(Al), leading to the formation of an antisite defect in the bcc lattice, thereby, increasing the chances of like atoms being the nearest neighbours. Thus, an atom occupying the wrong atomic site is possible. Such an arrangement of atoms causes the free energy of Fe(Al) to rise. Thus, the solid solution becomes thermodynamically metastable and offers much less resistance to grain refinement during the processing. In Fig. 5(d) and (e), the peak is shifted to the lower Bragg angle during milling to 18 h time causing an expansion in lattice, whereas peak shift to higher Bragg angle for 28 h of milling time is followed by contraction in lattice parameter.

3.2 DSC

The DSC plot obtained for powder sample mechanically alloyed for 28 h duration is shown in Fig. 5(f). An exothermic peak is observed at 400°C. This is due to the reaction between Fe and Al which are not completely alloyed to form FeAl phase, this result is also consistent with the XRD data, and such DSC data have been reported earlier [17].

3.3 SEM

SEM micrographs of unmilled powder samples are shown in Fig. 6(a) and (b). The unmilled Fe powders were rounded while those of Al were elongated in shape. Figure 6(c)–(f) show the sequence of SEM micrographs obtained at different milling duration, they illustrate the morphology of the powder particles ball milled from half an hour to 27 h. The average size of the powders gradually decreased with increasing milling time; it is also observed that the particle size distribution is wider at a longer milling time. Welding and flattening of particles are observed during longer milling duration as seen from Fig. 6(d) to (f).

3.4 XRD results of annealed powder

The XRD pattern of annealed powder sample is shown in Fig. 7. The sample was mechanically alloyed as a result of 28 hrs of milling time and subsequently annealed at 450°C. Figure 7 indicates super lattice peaks (100 and 221) of higher intensity, an Al (111) peak of lower intensity and the fundamental peak (110) is narrow compared to the XRD

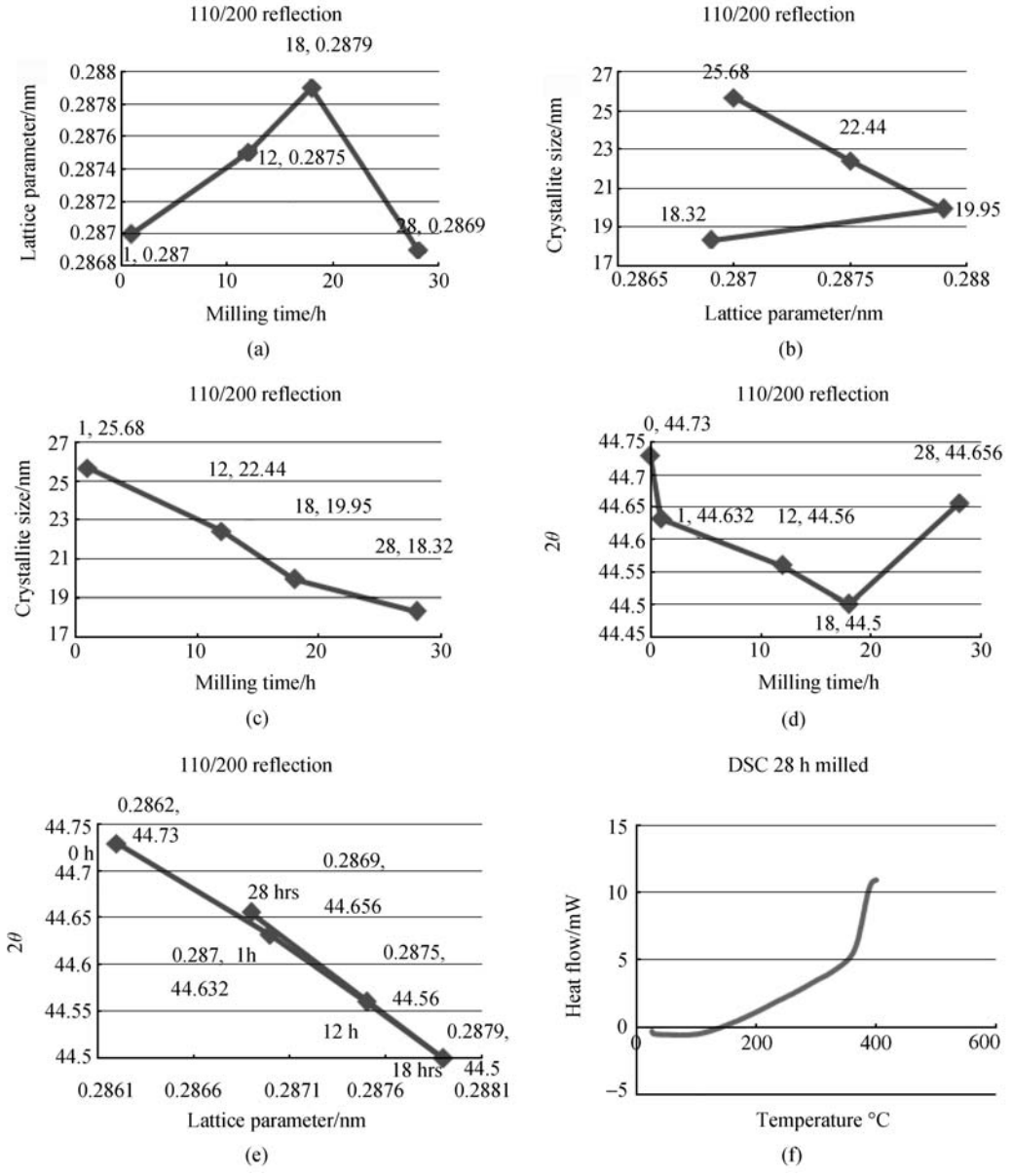

Fig. 5 **(a)** Lattice expansion occurs during 1 to 18 h of milling time, lattice contraction occurs during 18 to 28 h of milling time; **(b)** Crystallite size decreases from 25.68 to 19.95 nm during lattice expansion, while the decrease is from 19.95 to 18.32 nm during lattice contraction; **(c)** The crystallite size decrease is steep during 12 to 18 h of milling time; it is due to stabilisation of disorder; **(d)** The Bragg angle for the fundamental peak decreases from unmilled sample to 18 h milled sample, increase in Bragg angle occurs from 18 to 28 h of milling time; **(e)** The Bragg angle decreases during lattice expansion from 0.2862 to 0.2879 nm, while it increases during lattice contraction from 0.2879 to 0.2869 nm; **(f)** The DSC curve shows a rise in exothermic value from 180°C to a peak at 400°C

pattern of sample milled for 28 h (Fig. 4). These results indicate that the lattice becomes more ordered after annealing. High temperature diffusion of Al atoms into bcc FeAl lattice occurs and the grain size increases [19].

3.5 EDS

The SEM image in Fig. 8(a) shows the energy dispersive spectroscopy investigation on a particle mechanically alloyed for 18 h of time, approximately an average composition of Fe-50at.%Al is obtained as indicated in Table 2. The EDS analysis shows only Fe and Al peaks, and no tungsten and carbon peaks can be seen in Fig. 8(b), suggesting negligible contamination from the atmosphere and the milling media. EDS and XRD results are similar with respect to phase transformation, particle size and contamination, thus, showing consistency in the investigated results.

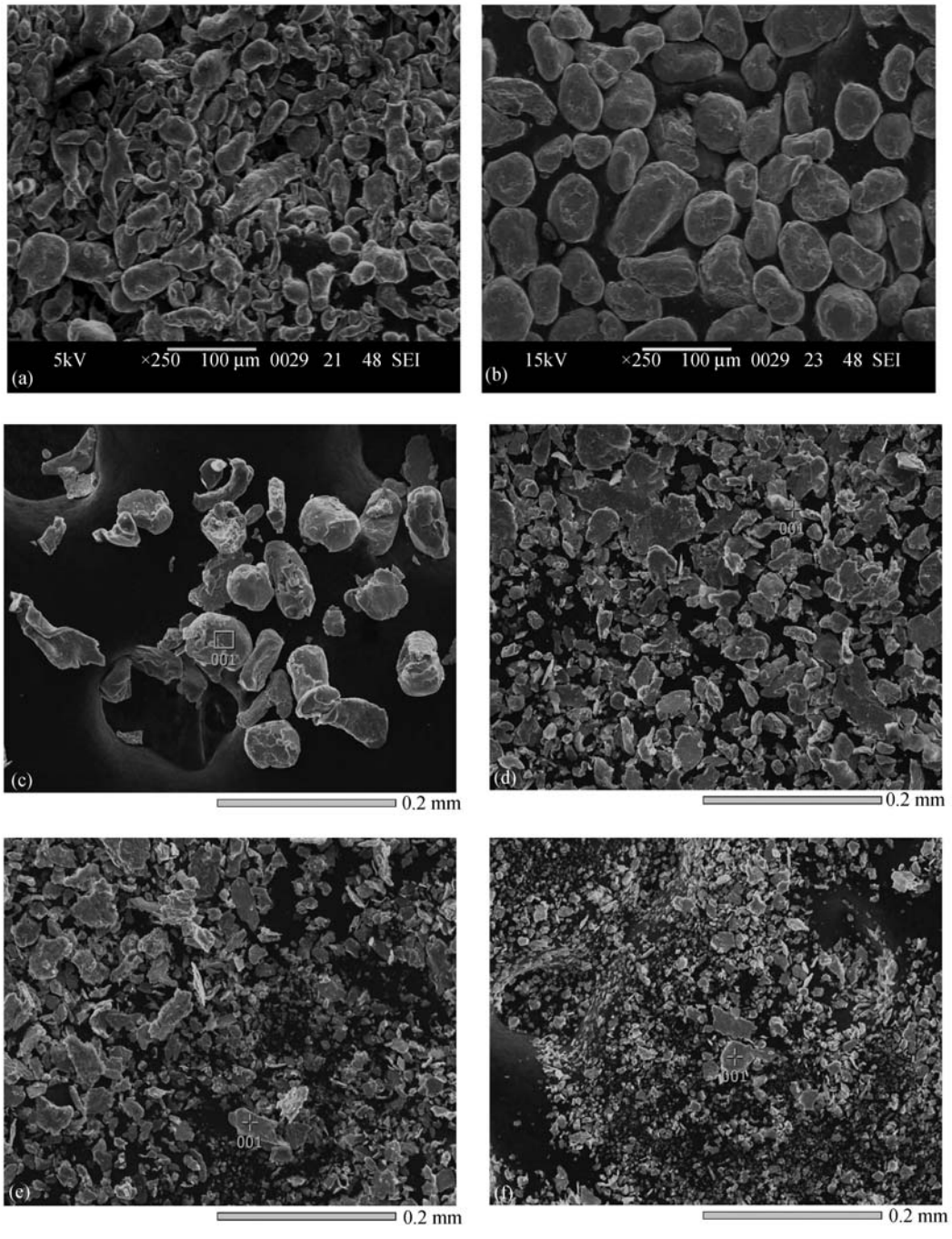

Fig. 6 SEM images: **(a)** unmilled Al powders; **(b)** unmilled Fe powders; **(c)** ball milled for 0.5 h; **(d)** ball milled for 4 h; **(e)** ball milled for 8 h; **(f)** ball milled for 27 h

3.6 Particle size measurement

The SEM image in Fig. 9 reveals the particle size of ball milled powders, micrograph shows 149 nm sized particle, obtained for a milling duration of 10 h. Particle of 673 nm size is seen in the micrograph shown in Fig. 10, a number of minute particles much smaller than the 673 nm sized particle are visible, and these results indicate particle size reduction with increased milling time, leading to the formation of nanosized particles at longer milling duration.

3.7 Micro hardness test

It is a well known fact that the introduction of atoms into the solid solution produces an alloy, which is stronger than the pure metal. Following this approach, it can be inferred

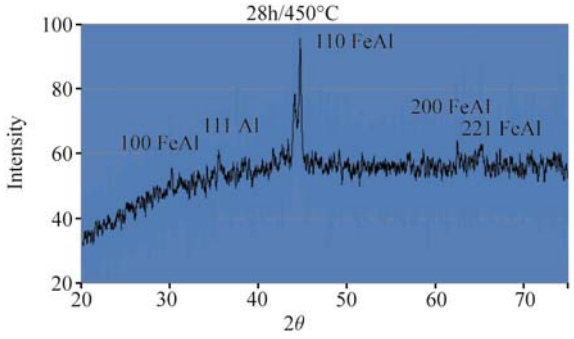

Fig. 7 XRD pattern of sample ball milled for 28 h of time and annealed at 450°C

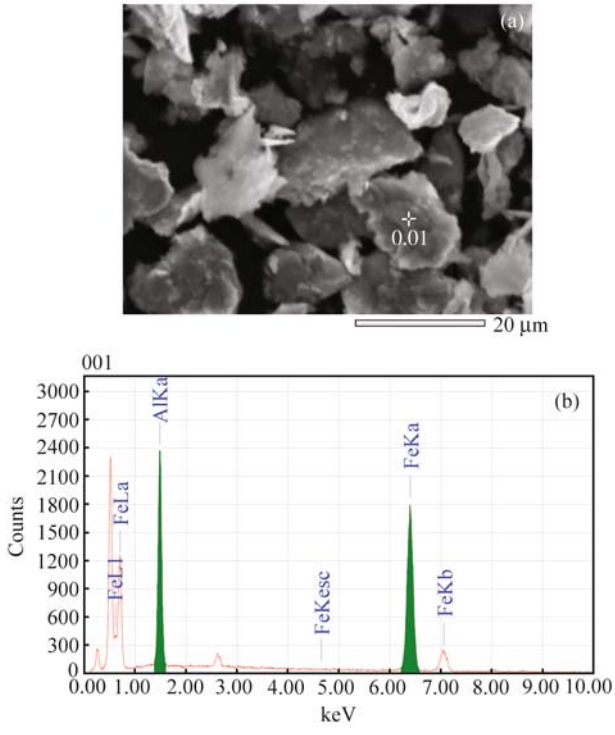

Fig. 8 **(a)** EDS micrograph shows spot analysis on a mechanically alloyed particle; **(b)** EDS graph indicates Fe and Al peaks

Table 2 Results of EDS performed using SEM on a mechanically alloyed particle

element	keV	mass%	error%	atomic%
Al Kα	1.486	29.43	0.17	46.33
Fe Kα	6.398	70.57	0.37	53.67
total	–	100	–	100

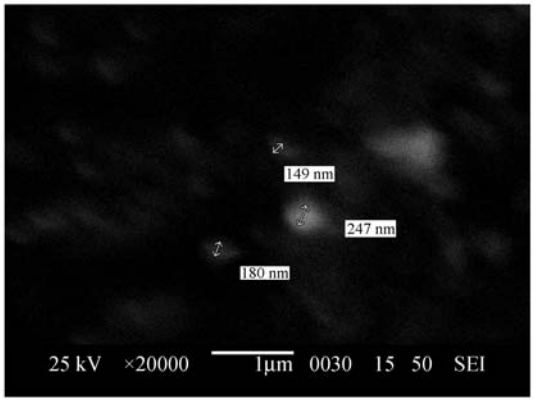

Fig. 9 SEM micrograph shows particle size measurement for 10 h milled sample

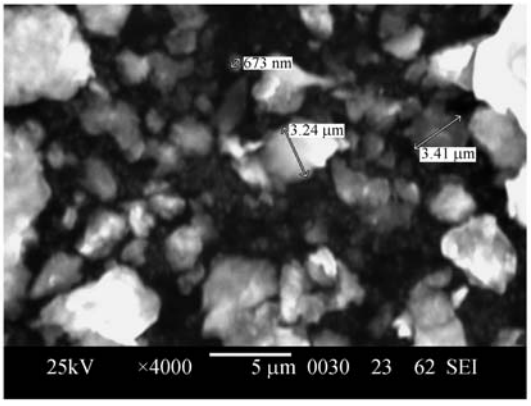

Fig. 10 SEM micrograph shows different particle sizes for a powder sample obtained at 24 h ball milling time

Table 3 Vickers micro hardness test results

milling time /h	hardness value /GPa	lattice parameter/nm	crystallite size, D	hkl reflection
0	5	0.2862	60–70 μm	110
1	5.24	0.2870	25.68 nm	110/200
12	6.46	0.2875	22.44 nm	110/200
18	7.55	0.2879	19.95 nm	110/200
28	7.84	0.2869	18.32 nm	110/200

that the mechanical properties of the mechanically alloyed intermetallics should be correlated to the induced structural changes, in particular, the disorder to order transition. From Table 3 and Fig. 11(a), it can be seen that the hardness increase is large during disordering (from 0 to 18 h of milling when lattice expansion occurs). The hardness increase is marginal during lattice contraction (from 7.55 to 7.84 GPa) as shown in Fig. 11(b). The lattice contraction during ordering is accompanied by a softening of the material. The softening is related to the marginal increase in hardness (from 7.55 to 7.84 GPa) and small reduction in crystallite size (from 19.95 to 18.32 nm) as a result of ball milling (Fig. 11(c)). These changes would be mainly controlled by the concentration of antisite defects present in the alloy. Micro hardness increases with grain size reduction. Hardness is not only enhanced by the disorder to order transition but also by the grain refinement. Amils et al. [15] and Varin et al. [20] have shown that the

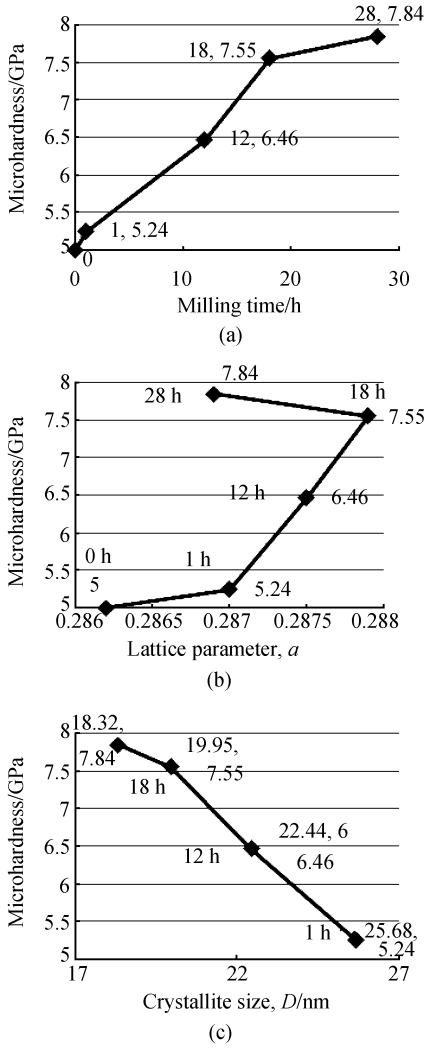

Fig. 11 **(a)** Micro hardness increases from 5.24 to 7.55 GPa during disordering while the increase from 7.55 to 7.84 GPa is due to ordering as a function of milling time; **(b)** Micro hardness increases from 5 GPa for unmilled sample to 7.84 GPa for 28 h milled sample, initial lattice expansion and final lattice contraction are observed with a marginal increase in hardness; **(c)** Hardness increases as crystallite size decreases, increase in hardness is small (from 7.55 to 7.84 GPa) during ordering and large during disorder

disordering process is characterized by an alloy hardening, which mainly depends on the grain refinement and the creation of antisite defects while the ordering process shows softening of the nanocrystalline alloy, which is governed by the annihilation of antisite defects.

4 Conclusions

Mechanically alloyed samples as a result of milling time for 18 h duration indicated the bcc Fe peak broadening, slight asymmetric formation, and shift to slightly lower Bragg angle. Simultaneously, the lattice parameter expanded, suggesting the formation of a new phase, the disordered bcc (FeAl). The contraction of lattice parameter, peak shift to higher Bragg angle and broadening, coupled with the presence of super lattice peak have shown the transition to an ordered FeAl phase for ball milling duration of 28 h. The LRO parameter obtained suggests a partial ordering of the mechanically alloyed sample for ball milling duration of 28 h. The ordered structure obtained is characterised by a small decrease in crystallite size compared to large decrease during disordering. Formation of nanocrystallites was confirmed by the XRD peak broadening and the XRD estimated nanocrystallite size decreased from 26 nm after 1 h to the 18 nm range after 28 h of milling. The presence of low intensity fcc Al peak along with the fundamental and super lattice peaks even after a substantially long milling time reveals that the process of MEA is still incomplete. The complete alloy phase (Fe(Al) or FeAl) formation is prolonged due to milling under toluene solution. The XRD results do not show DO3, tungsten and carbon peaks, suggesting negligible contamination from the atmosphere and the milling media.

XRD result of annealed powder shows more ordering, elevated temperature diffusion of Al into FeAl phase and grain enlargement.

The DSC result indicates the reaction between elemental Fe and Al, thus, elemental phase exists even after 28 h of MEA, and this result is also consistent with the XRD results.

The SEM micrographs show particle size reduction leading to nanoparticles during MEA as a function of milling time. EDS analysis on a mechanically alloyed particle show the atomic percentage of Fe and Al, thereby, confirming the formation of an alloy phase.

The hardness increase is large during disordering and marginal during ordering. Hardness is not only enhanced by the disorder to order transition but is also due to grain refinement.

Acknowledgements The authors would like to acknowledge Dr. Surappa and Shri Krishnamurthy from the Materials Department at the Indian Institute of Science (IISc), Bangalore for providing the XRD facility.

References

1. George E P, Baker I. Intermetallics: iron aluminides. In: Buschow K H J, Cahn R W, Flemings M C, et al, eds. The Encyclopaedia of Materials Science. Amsterdam: Elsevier, 2001, 4201–4205
2. Tortorelli P F, DeVan J H. Behavior of iron aluminides in oxidizing and oxidizing/sulfidizing environments. Materials Science and Engineering: A, 1992, 153: 573–577
3. Deevi S C, Sikka V K, Liu C T. Processing, properties, and applications of nickel and iron aluminides. Progress in Materials Science, 1997, 42: 177–192
4. Deevi S C, Sikka V K. Nickel and iron aluminides: an overview on

properties, processing, and applications. Intermetallics, 1996, 4: 357–375
5. Koch C C. The synthesis of non-equilibrium structures by ball-milling. Materials Science Forum, 1992, 88–90: 243–262
6. Suryanarayana C. Mechanical alloying and milling. Progress in Materials Science, 2001, 46: 1–184
7. Gleiter H. Materials with ultrafine microstructures: Retrospectives and perspectives. Nanostructured Materials, 1992, 1: 1–19
8. Suryanarayana C, Froes F H. The structure and mechanical properties of metallic nanocrystals. Metallurgical Transactions A, 1992, 23: 1071–1081
9. Nieman G W, Weertman J R, Siegel R W. Mechanical behavior of nanocrystalline metals. Nanostructured Materials, 1992, 1: 185–190
10. Siegel R W, Fougere G E. Mechanical properties of nanophase metals. Nanostructured Materials, 1995, 6: 205–216
11. Karch J, Birringer R, Gleiter H. Ceramics ductile at low temperature. Nature, 1987, 330: 556–558
12. McFadden S X, Mishra R S, Valiev R Z, et al. Low-temperature superplasticity in nanostructured nickel and metal alloys. Nature, 1999, 398: 684–686
13. Birringer R. Nanocrystalline materials. Materials Science and Engineering: A, 1989, 117: 33–43
14. Krasnowski M, Grabias A, Kulik T. Phase transformations during mechanical alloying of Fe-50%Al and subsequent heating of the milling product. Journal of Alloys and Compounds, 2006, 424: 119–127
15. Amils X, Nogues J, Surinach S, et al. Structural, mechanical and magnetic properties of nanostructured FeAl alloys during disordering and thermal recovery. Nanostructured Materials, 1999, 11: 689–695
16. Sebastian V, Lakshmi N, Venugopal K. Oxidation kinetics of the pack siliconized TiAl-based alloy and microstructure evolution of the coating. Intermetallics, 2007, 15: 1–7
17. Zeng Q, Baker I. Magnetic properties and thermal ordering of mechanically alloyed Fe-40at%Al. Intermetallics, 2006, 14: 396–405
18. Morris-Munoz M A, Dodge A, Morris D G. Structure, strength and toughness of nanocrystalline FeAl. Nanostructured Materials, 1999, 11: 873–885
19. Shi H W, Guo D B, Ouyang Y F. Structural evolution of mechanically alloy nanocrystalline FeAl intermetallics. Journal of Alloys and Compounds, 2007
20. Varin R A, Czujko T, Bystrzycki J, et al. Cold-work induced phenomena in B2 FeAl intermetallics. Materials Science and Engineering: A, 2002, 329–331: 213–221